THE JOURNAL OF PHYSICAL CHEMISTRY C

Article

pubs.acs.org/JPCC

Structural Information on the Au−S Interface of Thiolate-Protected Gold Clusters: A Raman Spectroscopy Study

Birte Varnholt,[†] Patric Oulevey,[†] Sandra Luber,[‡] Chanaka Kumara,[§] Amala Dass,[§] and Thomas Bürgi*[,†]

[†]Department of Physical Chemistry, University of Geneva, Quai Ernest Ansermet 30, 1211 Geneva, Switzerland

[‡]Department of Chemistry, University of Zurich, Winterthurerstrasse 190, 8057 Zurich, Switzerland

[§]Department of Chemistry and Biochemistry, University of Mississippi, 352 Coulter Hall, University, Mississippi 38677, United States

Supporting Information

ABSTRACT: The Raman spectra of a series of monolayer-protected gold clusters were investigated with special emphasis on the Au−S modes below 400 cm^{-1}. These clusters contain monomeric (SR-Au-SR) and dimeric (SR-Au-SR-Au-SR) gold−thiolate staples in their surface. In particular, the Raman spectra of $[Au_{25}(2\text{-PET})_{18}]^{0/-}$, $Au_{38}(2\text{-PET})_{24}$, $Au_{40}(2\text{-PET})_{24}$, and $Au_{144}(2\text{-PET})_{60}$ (2-PET = 2-phenylethylthiol) were measured in order to study the influence of the cluster size and therefore the composition with respect to the monomeric and dimeric staples. Additionally, spectra of $Au_{25}(2\text{-PET})_{18-2x}(S\text{-}/rac\text{-BINAS})_x$ (BINAS = 1,1′-binaphthyl-2,2′-dithiol), $Au_{25}(CamS)_{18}$ (CamS = 1*R*,4*S*-camphorthiol), and Au_nBINAS_m were measured to identify the influence of the thiolate ligand on the Au−S vibrations. The vibrational spectrum of $Au_{38}(SCH_3)_{24}$ was calculated which allows the assignment of bands to vibrational modes of the different staple motifs. The spectra are sensitive to the size of the cluster and the nature of the ligand. Au−S−C bending around 200 cm^{-1} shifts to slightly higher wavenumbers for the dimeric as compared to the monomeric staples. Radial Au−S modes (250−325 cm^{-1}) seem to be sensitive toward the staple composition and the bulkiness of the ligand, having higher intensities for long staples and shifting to higher wavenumbers for sterically more demanding ligands. The introduction of only one BINAS dithiol has a dramatic influence on the Au−S vibrations because the molecule bridges two staples which changes their vibrational properties completely.

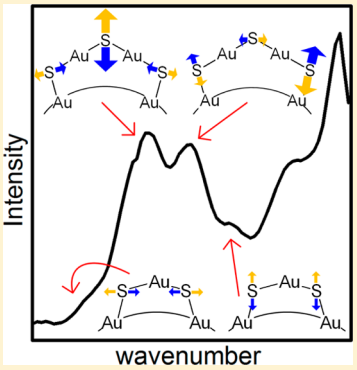

INTRODUCTION

Thiolate-protected gold nanoclusters are small particles of a well-defined structure consisting of a densely packed gold core surrounded by monomeric (SR-Au-SR) and dimeric (SR-Au-SR-Au-SR) gold−thiolate staples and sometimes other structural motifs.[1] They are an interesting system to study because of their size-dependent optical, chiroptical, and electronic properties.[2−6] Understanding the binding properties and structure of the Au−thiolate motifs, and the properties of the Au−S interface in general, is of importance for different research areas such as nanoelectronics and catalysis.[7,8] It has been demonstrated for example that the Au−S interface is quite flexible. Drastic rearrangements of the gold−thiolate staples on the cluster surface are possible at moderate temperatures as evidenced by the racemization of $Au_{38}(SR)_{24}$ and $Au_{40}(SR)_{24}$ clusters.[9,10] Also, adsorbed thiolates can place-exchange between different symmetry sites.[11]

Vibrational spectroscopy is a useful technique for studying gold clusters, particularly the structure of their Au−S interface. DFT calculations on small thiolate-protected gold clusters, with $[Au_{25}(SCH_3)_{18}]^-$ having been so far the biggest system considered, predict different far-infrared (FIR) and low-frequency Raman spectra for different cluster sizes.[12] For the $[Au_{25}(SCH_3)_{18}]^-$ cluster, the vibrations of the metal core (including its breathing mode) are predicted below 200 cm^{-1}, a S−CH_3 bending mode at 174 cm^{-1}, a Au−S stretching mode at 242 cm^{-1}, and the breathing mode of the staples at 269 cm^{-1}. Generally, the calculations predict a richer spectrum with more bands for Raman as compared to far-infrared.

Experimental Raman spectra were reported by Price and Whetten[13] for benzenethiolate-protected gold clusters of, at that time, unknown size and structure (1.5 and 1.7 nm clusters) and by Murray et al.[14] for the $[Au_{25}(2\text{-PET})_{18}]^{0/-}$ cluster (2-PET = 2-phenylethylthiolate). For the latter, a band around 300 cm^{-1} for the reduced and around 270 cm^{-1} for the neutral form was assigned to Au−S stretching modes. Recently, a systematic study on the FIR spectra of different 2-phenylethylthiolate-protected clusters was published.[15] Characteristic spectra for each size were recorded, but differences are subtle. A band at 490 cm^{-1} could be identified to indicate the conformation (gauche/trans) of the ligand. Heiz and co-workers[16] recently investigated the mid-infrared spectra of $[Au_{25}(2\text{-PET})_{18}]^{0/-}$, $Au_{38}(2\text{-PET})_{24}$, and $Au_{144}(2\text{-PET})_{60}$. No significant differences were found in the spectra of the different sizes besides a shift of the C−H stretching vibrations to lower frequencies for $[Au_{25}(2\text{-PET})_{18}]^{0/-}$. The spectrum of $Au_{144}(2\text{-PET})_{60}$ in the mid-infrared range was further analyzed in detail by Häkkinen and co-workers.[17] Line broadening in the crystalline state due

Received: March 11, 2014
Revised: April 3, 2014
Published: April 10, 2014

   dx.doi.org/10.1021/jp502453q | J. Phys. Chem. C 2014, 118, 9604−9611

to ligand-layer coupling was observed as compared to the cluster in solution.

To our knowledge, so far, no systematic study on Raman spectroscopy of the gold clusters was published. Complementary to our previous far-infrared study, here we present the Raman spectra of $[Au_{25}(2\text{-PET})_{18}]^{0/-}$, $Au_{38}(2\text{-PET})_{24}$, $Au_{40}(2\text{-PET})_{24}$, and $Au_{144}(2\text{-PET})_{60}$. Additionally, spectra of $Au_{25}(2\text{-PET})_{18-2x}(S\text{-}/rac\text{-BINAS})_x$ (BINAS = 1,1′-binaphthyl-2,2′-dithiol), $Au_{25}(CamS)_{18}$ (CamS = 1*R*,4*S*-camphorthiol), and Au_nBINAS_m were recorded to investigate the effect of the stabilizing ligand. Additionally we performed a calculation on $Au_{38}(SCH_3)_{24}$ in analogy to the series of small clusters calculated by Tlahuice et al.[12] for supplementary comparison with the experimental spectra.

METHODS

The synthesis and size separation of the different clusters were conducted following earlier reports,[18−22] and details can be found in the Supporting Information. All clusters were characterized by UV−vis spectroscopy and MALDI spectrometry to confirm purity (Supporting Information Figures S1−S3).

All spectra were measured on the SCP-ROA (scattered circular polarization−Raman optical activity) instrument developed by Hug and co-workers.[23,24] Measurements of Raman spectra of gold nanoclusters are nontrivial as the clusters are rather weak scatterers. They absorb strongly in the visible region, and thus the laser light at 532 nm used for excitation leads to strong local heating which can destroy the clusters. Therefore, a compromise between laser power and signal intensity had to be found. A laser light intensity of 8 mW was chosen while the sample, which was deposited on a glass plate, was rotated at about 3000 rpm to prevent the sample from decomposition from excessive heating. Measurements were performed in backscattering geometry. The mean spectral resolution is 7.8 cm^{-1}. This instrument with its fast optics and the detector with a very high sensitivity is advantageous for weakly scattering samples due to its high signal-to-noise ratio. Also, there was enough space in the focal region of the instrument to introduce a rotating sample holder.

In order to coat the glass (cover slides, 15 mm, MENZEL-Gläser), the clusters were dissolved in dichloromethane, and methanol was added for a lower surface tension leading to more homogeneous coating. To exclude artifacts, for the series of 2-PET stabilized clusters at least three glass cover slides per sample were prepared; each was measured at three different positions. For the other clusters, due to low sample amounts available, only one glass slide was prepared and measured in three different positions.

The spectra obtained show small signals on top of a strong background which has several origins, the most important being fluorescence, back-reflections of scattered light from the sample holder, and the spectrum of the glass support. An example of a raw spectrum is shown in the Supporting Information (Figure S4). The background is poorly reproducible due to differences in coating and different sample positions. No simple subtraction or fitting method could satisfactorily remove the background. Therefore, we opted for a rolling circle filter (RCF).[25] First, an adequate diameter of the circle had to be found. Two main criteria should be met: The diameter must be significantly larger than the width of a Raman band (or overlapping neighboring bands). Additionally, the circle has to be smaller than the usually broad background features. The broadest band in the spectrum is around 100 cm^{-1} wide; the background features are wider (>200 cm^{-1}).

For practical reasons, the spectrum is converted into a quadratic matrix in dimensionless space. The resolution of the spectrum is slightly wavelength dependent and corresponds in mean to 2.3 cm^{-1} per pixel; hence, a width of 100 cm^{-1} corresponds to about 43 points. To prevent the circle from entering the bands of interest, we chose a diameter of 80 points.

Further, a cutoff parameter below which the spectrum was discarded had to be chosen. This is necessary to prevent the circle to be held back at the steep optical filter flank which would result in an incomplete removal of the background for low wavenumbers. The cutoff parameter was set at 163 cm^{-1}.

Additionally, we chose to interpolate linearly between the measured points. The reason for this is the low horizontal resolution of the CCD detector, which otherwise determines (without interpolation) the number of elements of the quadratic matrix. The shape of the circle formed with such a low number of points (at the original spectral resolution) would not be a smooth arc; the resulting polygon shape could not remove the background completely. We chose to interpolate linearly with 20 points between each spectral data point. All spectra were treated with the same parameters to ensure good comparability of the spectra. After applying the described filtering procedure to remove the broad background features, the spectra were well reproducible for different samples of the same cluster and at different positions on the same glass slide.

To facilitate band assignment, the Raman spectrum of the $Au_{38}(SR)_{24}$ cluster was calculated. The structure of the cluster was optimized with the program package TURBOMOLE,[26] version 6.4, by means of density functional theory (DFT). Because of the very high computational effort, all 2-PET ligands in the structure were replaced by methylthiolate groups and a small basis set, SV(P),[27,28] had to be chosen. Furthermore, a quasirelativistic pseudopotential[29] was employed for the Au atoms. Since the BP86 density functional[30,31] has been found to perform well in static frequency calculations,[32−35] it was used in all calculations together with the corresponding auxiliary basis sets[28,36] needed for the resolution-of-the-identity density-fitting approximation.[37,38] The quantities to predict the Raman spectrum were calculated in the double-harmonic approximation[39,40] employing the MOVIPAC[41] program package in combination with electronic energy gradients and the electric-dipole−electric-dipole polarizability tensor α obtained from TURBOMOLE. (For sake of brevity, we will refer to the electric-dipole−electric-dipole polarizability simply as polarizability in the following.)

Turbomole's ESCF module[38,42,43] was utilized for the computation of the static polarizability. The second derivatives of the electronic energy with respect to the nuclear coordinates were calculated numerically by MOVIPAC[41] via a 3-point central difference formula.[44] The step length in the numerical differentiation was set to 0.01 bohr.

The predicted Raman spectrum was obtained from the current development version of PyVib2-2.0,[45] soon to be released, by combining the quantities obtained from MOVIPAC, i.e., the Cartesian displacement vectors L_x and the Cartesian gradients of α.[46] The bands were plotted using six Gaussians with isotropic and anisotropic fwhm of 3.5 and 10.0 cm^{-1}, respectively. The same program was used to visualize selected normal modes in their atomic excursion representation.[46]

dx.doi.org/10.1021/jp502453q | J. Phys. Chem. C 2014, 118, 9604−9611

RESULTS AND DISCUSSION

Our instrument is able to measure a spectral range of 170−2400 cm^{-1}. Therefore, we can study Au−S related vibrations on which we will have a closer look, and vibrations of the ligand residue which are largely unaffected by the cluster size and thus of smaller interest. Nevertheless, sharp bands at 1600, 1210, and 1000 cm^{-1} associated with a combination of C−H ring bending and wagging modes[47] can serve as reference to estimate relative intensities.

Influence of the Size and Structure for Clusters with the Same Ligand. The structures of the anionic and the neutral form of the cluster $Au_{25}(2\text{-PET})_{18}$ were obtained by single crystal X-ray diffraction (XRD). An icosahedral gold core (Au_{13}) is surrounded exclusively by six dimeric gold−thiolate units with some distortions in the reduced form, probably due to the presence of the counterion in the crystal.[48] The structure of $Au_{38}(2\text{-PET})_{24}$ is also known from single crystal XRD. A bi-icosahedral Au_{23} core is covered with six dimeric units (three at each pole) and three monomeric units (at the equator).[49] So far, no crystal structure of $Au_{40}(2\text{-PET})_{24}$ could be obtained. However, DFT calculations were performed. Häkkinen and co-workers published a structure based on a core built of two icosahedra with four long and six short staples.[50] Another theoretical structure was recently published by Jiang.[51] According to this, the core is protected by six long and three short units. The structure of $Au_{144}(2\text{-PET})_{60}$ was predicted by Häkkinen et al.[52] An Au_{114} core is protected by 30 monomeric gold−thiolate units.

Our series contains clusters protected only by long units ($Au_{25}(2\text{-PET})_{18}$), only by short units ($Au_{144}(2\text{-PET})_{60}$), and mixed shells ($Au_{38}(2\text{-PET})_{24}$ and $Au_{40}(2\text{-PET})_{24}$). Additionally to the different cluster sizes, the spectrum of the free ligand was measured (in liquid phase contained in a capillary) as well, so contributions of the ligand to the bands assigned as gold−sulfur interactions can be excluded. The low-frequency region, in which gold−sulfur vibrations are expected, is shown in Figure 1. Note that the Raman spectrum of the counterion of $Au_{25}(2\text{-PET})_{18}^{-}$, tetraoctylammonium, has no prominent bands in the region below 600 cm^{-1}.

The 50% transmission point of our RazorEdge filter (Semrock) used to block the exciting light lies in the vicinity of 150 cm^{-1}. Because of the steepness of the filter, the band of lowest wavenumber we can observe is the Au−S−C bending at 175 cm^{-1}, which was also reported by Murray et al.[14] in the Raman spectra of $Au_{25}(2\text{-PET})_{18}$, although with low observed relative intensity. In the FIR-spectra the band is present for all investigated sizes except for $Au_{40}(2\text{-PET})_{24}$. In the present study the intensity and position of this band should be considered with caution because our optical filter cutoff range presumably partially superimposes on this band, and thus peak maxima—affecting exact knowledge of the position and intensity—remain ambiguous. Another band assigned to Au−S−C bending is observed in the range 195−215 cm^{-1} for all clusters (Figure 1). The band shifts to higher wavenumbers with decreasing cluster size (more long staples). Further, the intensity of this band with respect to the three characteristic ligand bands mentioned above also varies. Higher intensities are observed for the mixed shell clusters $Au_{38}(2\text{-PET})_{24}$ and $Au_{40}(2\text{-PET})_{24}$. However, the intensities in the spectral range around 200 cm^{-1} and below may be affected by the background and its subtraction method, and therefore conclusions drawn from the band intensities in this region should be taken with caution.

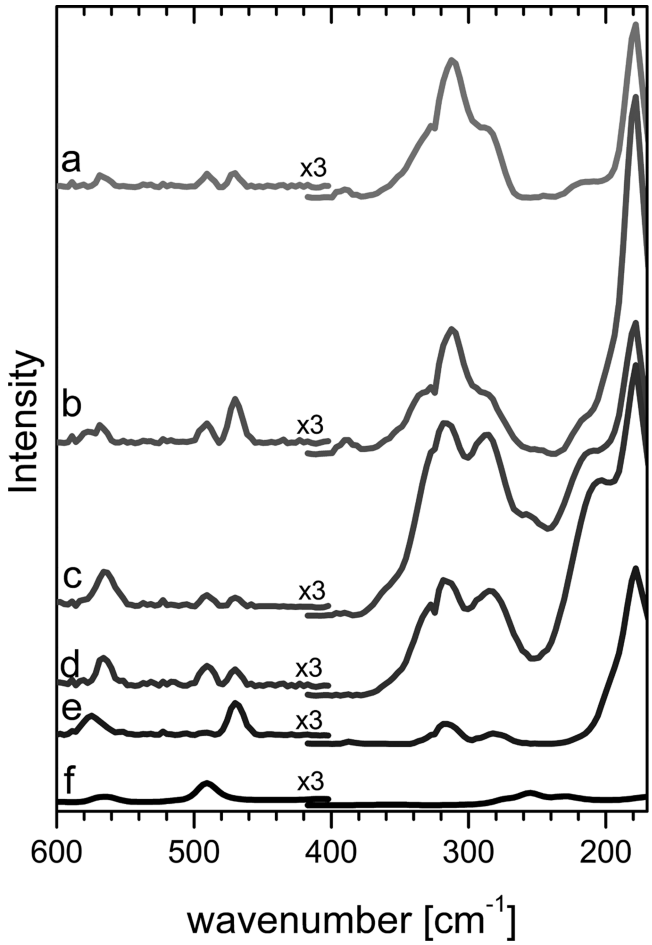

Figure 1. RCF corrected Raman spectra of the low-frequency region of $Au_{25}(2\text{-PET})_{18}^{0}$ (a), $Au_{25}(2\text{-PET})_{18}^{-}$ (b), $Au_{38}(2\text{-PET})_{24}$ (c), $Au_{40}(2\text{-PET})_{24}$ (d), $Au_{144}(2\text{-PET})_{60}$ (e), and the free ligand 2-PET (f). The spectra of the clusters were normalized to laser power and measuring time. However, absolute intensities cannot be directly compared because of irreproducible thickness of the coating. The spectrum of the free ligand was scaled in a way that the ligand vibrations, namely the sharp and intense bands at 1000 and 1600 cm^{-1}, have comparable intensities. For higher wavenumbers, the full spectra are reproduced in the Supporting Information (Figure S5).

Two types of Au−S stretching vibrations can be distinguished: tangential and radial modes. The latter involves movements of the thiolate against the cluster surface, thus involving Au(core)−S bonds. The staple breathing mode, where all staples in phase increase and decrease their distance to the Au core, represents a special case of radial modes and is strongly Raman active. In contrast, the tangential modes, which are weakly Raman active, involve movements of the thiolates parallel to the cluster surface where mostly Au(staple)−S bonds are involved.

Theoretical calculations by Tlahuice et al. predict both radial and tangential Au−S vibrations between 220 and 350 cm^{-1}—the latter at higher wavenumbers and with very low intensities.[12] In the experimental spectra (Figure 1) it can be clearly seen that the ligand shell strongly influences the bands at 281−289 and 309−317 cm^{-1}. Note that the small dip at 330 cm^{-1} is due to the support and does not enter into the following discussion.

dx.doi.org/10.1021/jp502453q | J. Phys. Chem. C 2014, 118, 9604−9611

The largest system considered by Tlahuice et al. is the $Au_{25}(2\text{-PET})_{18}$ anion cluster—our smallest investigated cluster. Its experimental Raman spectrum (Figure 1b) can directly be compared to the Raman spectrum calculated by DFT.[12] One has to bear in mind though that in the calculations the S−CH_3 ligand was used, whereas in the experiment the 2-PET ligand was present, which could lead to changes in the spectra due to the different reduced masses of the normal modes and steric effects (see below). The calculated Raman spectrum in the considered frequency range is dominated by two bands around 270 and 240 cm^{-1} consisting of several superimposed modes. The former band contains the special case of the breathing mode which is expected to have a high Raman intensity due to the large change in the clusters polarizability. Comparison with the experimental spectrum seems to indicate that the corresponding bands are found at around 320 and 280 cm^{-1} in the experiment, with the former being the most intense band.

We calculated the vibrational spectrum of $Au_{38}(SCH_3)_{24}$. Figure 2 shows the Raman spectrum of the low wavenumber range and a schematic presentation of characteristic vibrations. The structure of the cluster is shown in Figure 3a; the representative normal modes in the excursion representation (Figure 3b−f) correspond to the highlighted staples. An assignment of bands is provided in Table 1.

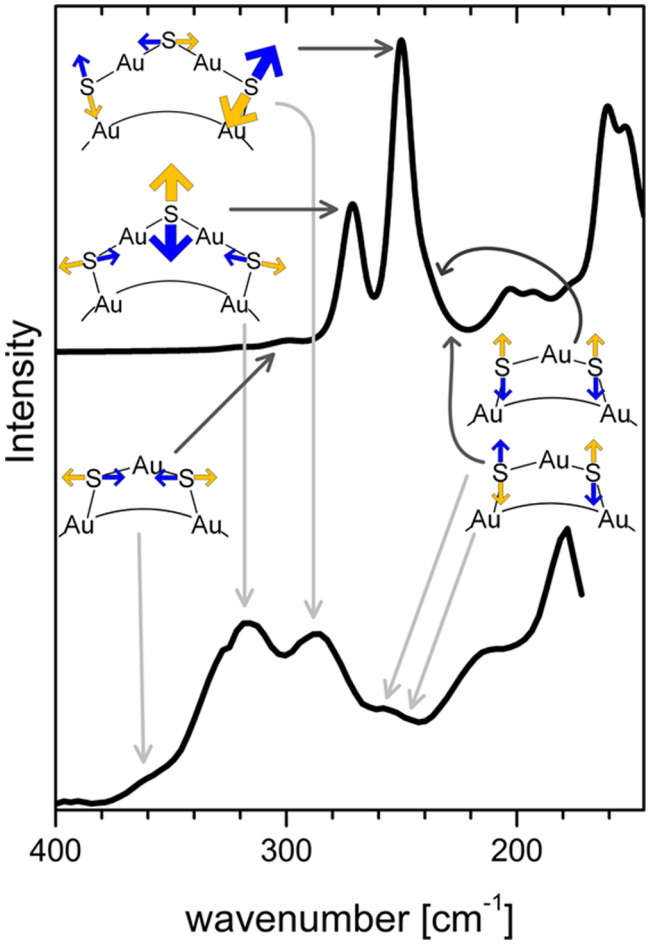

Figure 2. Calculated (top) and experimental (bottom) Raman spectrum of the $Au_{38}(SCH_3)_{24}$ and $Au_{38}(2\text{-PET})_{24}$ cluster, respectively. The experimental spectrum is cut off at 170 cm^{-1}, the cutoff point of our optical filter. Radial and tangential Au−S modes of the staples are schematically represented. Radial vibrations of the long staples are responsible for bands with high intensity. Modes associated with the short staples (symmetric and antisymmetric stretching and tangential vibrations) have lower Raman intensity.

The calculated spectrum is quite similar to the one of $Au_{25}(SCH_3)_{18}^-$. Bands around 175 and 200 cm^{-1} belong to Au−S−C bending modes. As discussed above, the latter band is sensitive toward the staple type. Vibrations of short staples appear at lower energies; bending of long staples requires higher energy. This is in accordance to the experimental results; the band for $Au_{144}(2\text{-PET})_{60}$ lies at 195 cm^{-1}, and a shift of 20 cm^{-1} is observed for $Au_{25}(2\text{-PET})_{18}$, which shows a band at 215 cm^{-1}. The tangential vibrations (Figure 3f) have a very low Raman cross section and are predicted slightly below 300 cm^{-1}. The bands of highest intensity between 240 and 280 cm^{-1} are characteristic for the staple type as well. The short S−Au−S staples in the equatorial region of the cluster experience antisymmetric (Figure 3b) and symmetric (Figure 3c) radial stretching. In the theoretical spectrum, the former occur around 230 cm^{-1} with a relatively low Raman intensity. The symmetric stretching causes a larger change in polarizability which is associated with a larger Raman intensity. The observed band is a superposition of the mostly isolated vibrations of the three short staples and is observed as a shoulder of the intense band due to the long staples.

The most intense predicted band around 250 cm^{-1} is associated with a stretching of the Au(core)−S bond of the long staple. Mainly the sulfur at the "pole side" of the staple moves; the Au(core)−S bond closer to the equator stretches only slightly (Figure 3d). The band at 276 cm^{-1} is assigned to a vibration of long staples perpendicular to the surface (radial mode). Here, mainly the sulfur in the center of the staple moves (Figure 3e); those bound to the gold core experience only a small deflection. The sulfur's free electron pairs cause a strong change of polarizability during the radial reflection, which explains the high intensity of the corresponding bands. The general shape of the experimental spectrum of $Au_{38}(2\text{-PET})_{24}$ is reproduced by the calculations of $Au_{38}(SCH_3)_{24}$. The two dominating bands consisting of the above-discussed radial vibrations of short and long staples correlate to those of highest intensity in the experimental spectrum at 285 and 316 cm^{-1}. Additionally, the weak bands belonging to the tangential vibrations can be observed as a shoulder from 340 to 360 cm^{-1}. The discrepancy between wavenumbers in the calculated and experimental spectrum has likely two main reasons: Instead of the 2-PET ligand used in the experiment, the calculations were performed with methylthiolate; additional experiments with different ligands (see below) show that the different ligand structure can be responsible for a wavenumber shift. Further, due to the extensive size of the system, a small basis set was used, which affects the accuracy of predicted normal-mode frequencies (besides other approximations made in the calculation such as a temperature of 0 K and the neglect of the environment, anharmonic contributions, and certain relativistic corrections).

The spectra of $Au_{25}(2\text{-PET})_{18}^{0/-}$ and $Au_{38}(2\text{-PET})_{24}$ are quite similar, both experimentally and calculated. The reason for this is likely the presence of long staples on both clusters, which, according to the calculations, dominate the Raman intensities.

The spectrum of $Au_{40}(2\text{-PET})_{24}$ is comparable to the one of $Au_{38}(2\text{-PET})_{24}$. Both clusters have a mixed shell with short and long staples. All bands lie at similar wavenumbers and have similar intensity.

dx.doi.org/10.1021/jp502453q | J. Phys. Chem. C 2014, 118, 9604−9611

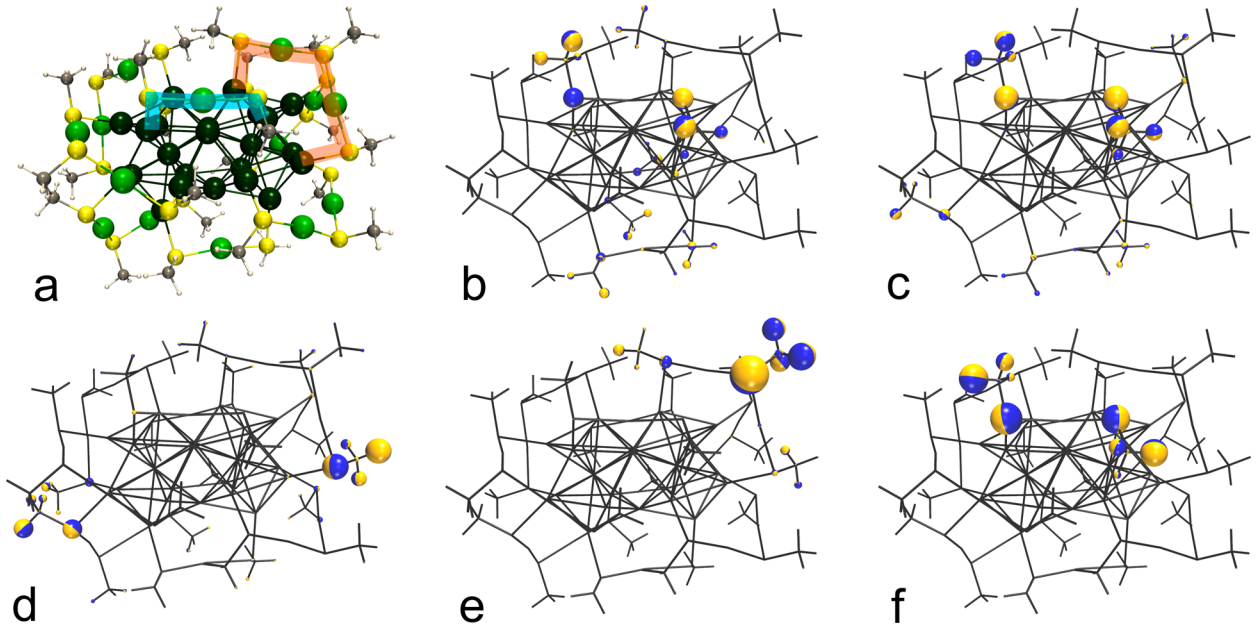

Figure 3. Illustration of the structure of the $Au_{38}(SCH_3)_{24}$ cluster (core gold atoms: dark green, staple gold atoms: light green, sulfur: yellow, carbon: gray, hydrogen: white; one short and one long staple are emphasized in blue and orange, respectively) (a) and characteristic Au−S vibrations: antisymmetric radial stretching of short staples (b: 233 cm^{-1}), symmetric stretching of short staples (c: 244 cm^{-1}), radial vibration of the outer sulfur of the long staples (d: 248 cm^{-1}), radial vibration of the center sulfur of the long staples (e: 276 cm^{-1}), and tangential vibration of the short staples (f: 292 cm^{-1}). Displacements of atoms are perpendicular to the circular plane defined by the two hemispheres, and the diameter of the sphere is proportional to the atomic excursion.

Table 1. Assignments of the Calculated and Experimental Raman Bands in the Low Wavenumber Range for $Au_{38}(SCH_3)_{24}$ and $Au_{38}(2\text{-PET})_{24}$, respectively[a]

$Au_{38}(SCH_3)_{24}$ calc	$Au_{38}(2\text{-PET})_{24}$ exp	assignment
175	178	Au−S−C bending
193	208	Au−S−C bending—mostly located on short staples
203	208	Au−S−C bending—mostly located on long staples
235		antisymmetric radial stretching of short staples
244	257	symmetric stretching of short staples
250	286	radial vibration of the outer sulfur of the long staples
271	316	radial vibration of the center sulfur of the long staples
298	357	tangential vibration of the short staples

[a]The given wavenumbers correspond to the maximum of the bands which are a superposition of the different staples with the same symmetry. Contrary to this, the wavenumbers we refer to in Figure 3 correspond to the vibrations of chosen staples.

For $Au_{144}(2\text{-PET})_{60}$, the Au−S−C bending at 195 cm^{-1} is shifted to significantly lower wavenumbers as compared to the other cluster sizes. The cluster contains only short staples whose bending is predicted at lower wavenumbers as compared to long staples. The bands at 280 and 320 cm^{-1} have a lower relative intensity with respect to the Au−S−C bending vibration at 175 cm^{-1} and to the reference bands of ligand vibrations when compared to the other clusters studied. This finding can also be explained by the absence of dimeric staples whose radial vibration is the origin of the strong bands around 300 cm^{-1} for the other clusters. The weaker bands in this region are assigned to radial vibrations of short staples which generally have a lower Raman intensity than those of the long staples.

We previously discussed[15] the influence of the ligand conformation (trans/gauche) on the infrared spectrum at 490 cm^{-1}. Calculations showed that this band, which arises from phenyl out-of-plane (oop) deformation coupled with C−C−S bending modes, is present for trans conformations, whereas the 470 cm^{-1} component can be attributed to the gauche conformation and a coupling of phenyl oop deformation with C−S torsion. Although different in relative intensity, both bands were present for all cluster sizes in the FIR study. Contrary to this, the Raman spectra show strong differences. The bands assigned to gauche and trans conformations have roughly the same intensity for the clusters $Au_{25}(2\text{-PET})_{18}^{0}$, $Au_{38}(2\text{-PET})_{24}$, and $Au_{40}(2\text{-PET})_{24}$. The reduced form of $Au_{25}(2\text{-PET})_{18}$ has a more intense gauche band than trans, and $Au_{144}(2\text{-PET})_{60}$ has exclusively a signal for the gauche conformation. It should be noted that the sample preparation might play a role for the conformation of the ligands, which is not necessarily the same in the dried films and the crystal structure.

Influence of the Ligand for Clusters of the Same Size. The $Au_{25}(SR)_{18}$ cluster was chosen as a system to investigate the influence of the ligand on the Au−S vibrations. Additionally to the above-discussed $Au_{25}(2\text{-PET})_{18}^{0/-}$ we also investigated the 1*R*,4*S*-camphorthiol (CamS) stabilized cluster and further exchanged both the neutral and reduced 2-PET stabilized cluster with *S*- and *rac*-BINAS. The clusters exchanged with BINAS were further compared to purely BINAS protected clusters of an unknown size. The synthesis procedures were described earlier.[21,22,53]

For the camphorthiol-stabilized cluster, the Au−S−C bending at 178 and 212 cm^{-1} are remarkably unchanged in frequency compared to the previously discussed 2-PET cluster

dx.doi.org/10.1021/jp502453q | J. Phys. Chem. C 2014, 118, 9604−9611

(Figure 4). The steric effect of the ligand and the different mass do not appear to have a (large) impact on these vibrations.

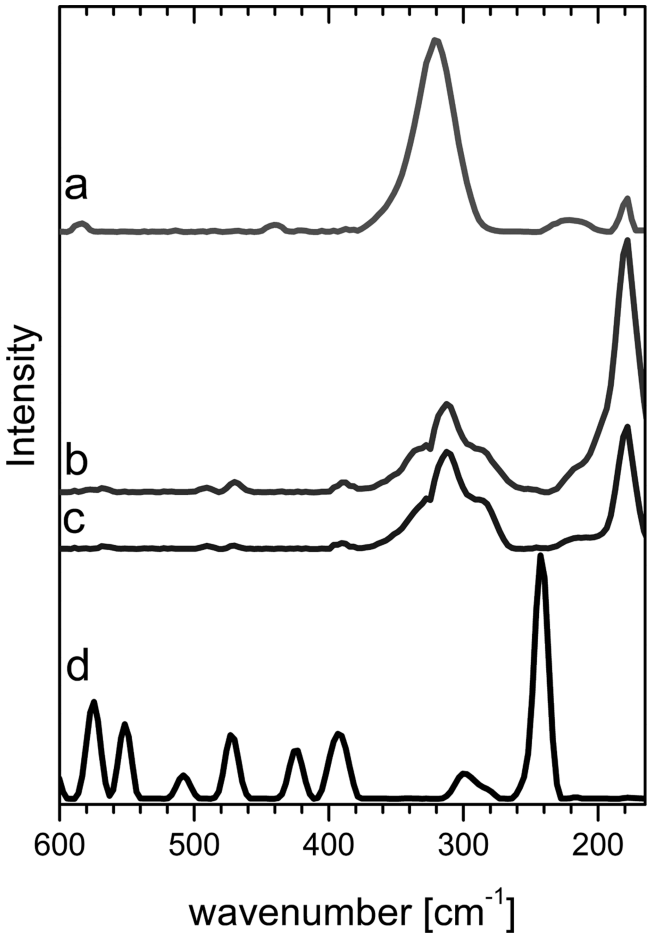

Figure 4. RCF-corrected Raman spectra of the low-frequency region of $Au_{25}(CamS)_{18}$ (a), $Au_{25}(2\text{-}PET)_{18}^{0}$ (b), $Au_{25}(2\text{-}PET)_{18}^{-}$ (c), and free ligand CamSH (d). The clusters were measured coated on a rotating glass slide; the free ligand was measured in solid state in a rotating glass capillary. The latter allowed higher quantities and higher laser power, resulting in a stronger spectrum, which was downscaled for comparison.

Contrary to this, the intense radial vibrations are shifted to higher wavenumbers and superimpose; the distinct bands characteristic of the $Au_{25}(2\text{-}PET)_{18}^{0/-}$ cluster are not observed anymore. At first thought one may expect a shift to lower wavenumbers because of the higher mass of camphorthiol compared to 2-PET. The shift to higher wavenumbers can be explained with steric hindrance. The movement gets more difficult the bulkier the ligand is, because in these vibrations the ligands move partly against each other.

Note that the spectrum of the free ligand does not overlay with Au−S vibrations, and therefore the observations described above are not disturbed by the spectrum of the ligand.

The ligand exchange of $Au_{25}(2\text{-}PET)_{18}^{0/-}$ with *S*- and *rac*-BINAS leads to species of the composition $Au_{25}(2\text{-}PET)_{18-2x}(S\text{-}/rac\text{-}BINAS)_x$ with mainly $x = 1$ for the neutral form and $x = 2$ for the reduced cluster; their Raman spectra are shown in Figure 5. The difference in the number of exchanged ligands is possibly due to a different excess ratio of BINAS with respect to the cluster in the exchange experiment as the exact concentration of the cluster was unknown. The clusters show

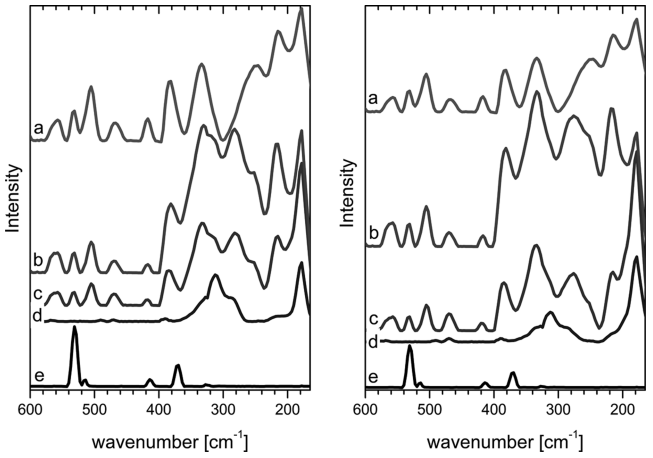

Figure 5. RCF-corrected Raman spectra of the neutral (left) and the reduced (right) form of $Au_{25}(2\text{-}PET)_{18-2x}(rac\text{-}BINAS)_x$ (b), $Au_{25}(2\text{-}PET)_{18-2x}(S\text{-}BINAS)_x$ (c), $Au_{25}(2\text{-}PET)_{18}$ (d), the reference spectrum of the free ligand *S*-BINAS (e), and a purely *S*-BINAS protected Au-cluster of not yet determined size (a).

the same number for *S*- and *rac*-BINAS for each oxidation state as the same stock solution was used here.

For these clusters the band corresponding to Au−S−C bending experiences a slight shift to higher wavenumbers (218 cm^{-1}) and is generally more defined and higher in intensity. Apart from this, assignments are difficult without additional theoretical calculations.

It seems that the bands at 282 and 315 cm^{-1} observed in the $Au_{25}(2\text{-}PET)_{18}^{0/-}$ cluster are maintained; the latter is now only visible as a shoulder of a rising Au-BINAS band. All other bands are similar to the spectrum of the purely BINAS stabilized cluster of unknown size. Subtle differences can further be observed between the spectra of the two oxidation states; mainly the bands at 282 and 315 cm^{-1} are better defined for the neutral form. This is likely due to the lower number of exchanged ligands. These findings are supported by UV−vis spectra, which are less defined for the exchanged species of the reduced form, and the "circular dichroism (CD) spectra, which is stronger for the reduced form (Supporting Information Figure S2).

Basically no differences can be observed between the spectra of the clusters exchanged with *S*-BINAS and *rac*-BINAS for the same oxidation state, which can also be regarded as a confirmation of the reproducibility of the applied procedures. The general higher intensity in the latter case can be explained by a thicker coating on the glass, which led to higher intensities. The presence of molecules with the same or with opposite handedness on the same cluster may lead to different spectral signatures, which is however not observed here.

It is apparent that the introduction of BINAS to the $Au_{25}(2\text{-}PET)_{18}^{0/-}$ cluster has a tremendous effect on the Au−S vibrations. This is astonishing as on average only one (neutral form) or two (reduced form) BINAS molecules are introduced on the surface. The drastic change in the spectrum is ascribed to the binding properties of the BINAS ligand. The bidentate thiol is expected to bridge staple units,[22,54] thereby causing a distortion of the Au−S protecting units and rendering the Au−S interface more rigid.[55] This seems to have a drastic effect on the normal modes localized on the Au−S bonds.

dx.doi.org/10.1021/jp502453q | J. Phys. Chem. C 2014, 118, 9604−9611

CONCLUSION

This report presents a systematic study of Raman spectra for different sizes of the well-known 2-PET protected gold clusters. With the help of previously reported calculations on $Au_{25}(2\text{-PET})_{18}$ and new calculations on the $Au_{38}(2\text{-PET})_{24}$ cluster, the Au−S−C bending and the radial Au−S vibrations were identified to reveal information on the surface structure of gold clusters. It is evident that the type and number of gold−thiolate binding units influence the spectrum. Experimentally, the bending vibrations lie at 195 cm^{-1} for monomeric staples and are shifted to 215 cm^{-1} for dimeric staples. This shift is reproduced by the calculation. Clusters with mixed shells show a band in between these values. The shift seems to be largely independent of the ligand type.

The radial vibrations are also sensitive to the surface structure, but no clear trend could be identified in the experimental spectra to differentiate between monomeric and dimeric staples. However, a shift to higher wavenumbers is seen for sterically demanding ligands. The shape of the calculated spectrum of $Au_{38}(SCH_3)_{24}$ corresponds well with the experimental spectrum of $Au_{38}(2\text{-PET})_{24}$. It seems that the long staples dominate the Raman intensity of the Au−S vibrations of the clusters. The Raman spectrum of the Au−S interface is furthermore extremely sensitive to the introduction of a dithiol to the ligand shell. Exchange of two monothiols by only one dithiol changes the Raman spectrum completely, which is likely due to the bridging of staples.

ASSOCIATED CONTENT

Supporting Information

Structure of the ligands; synthetic details and characterization of all investigated clusters (UV−vis and MALDI spectra); illustration of the background removal procedure; full wavenumber range of all Raman spectra. This material is available free of charge via the Internet at http://pubs.acs.org.

AUTHOR INFORMATION

Corresponding Author

*E-mail thomas.buergi@unige.ch; tel ++41 22 379 65 52 (T.B.).

Notes

The authors declare no competing financial interest.

ACKNOWLEDGMENTS

Financial support from the Swiss National Science Foundation and the University of Geneva is kindly acknowledged. We thank Prof. Stefan Matile for providing the CD spectrometer and Sophie Michalet for MALDI measurements. We are grateful to Stefan Knoppe for providing the 1*R*,4*S*-camphorthiol and to Raymond Azouley for the synthesis of 1,1′-binaphthyl-2,2′-dithiol. A.D. and C.K. gratefully acknowledge support from NSF 0903787 and the international travel grant.

REFERENCES

(1) Häkkinen, H.; Walter, M.; Grönbeck, H. Divide and Protect: Capping Gold Nanoclusters with Molecular Gold-Thiolate Rings. *J. Phys. Chem. B* **2006**, *110*, 9927−9931.

(2) Negishi, Y.; Nobusada, K.; Tsukuda, T. Glutathione-Protected Gold Clusters Revisited: Bridging the Gap between Gold(I)-Thiolate Complexes and Thiolate-Protected Gold Nanocrystals. *J. Am. Chem. Soc.* **2005**, *127*, 5261−5270.

(3) Lopez-Acevedo, O.; Tsunoyama, H.; Tsukuda, T.; Häkkinen, H.; Aikens, C. M. Chirality and Electronic Structure of the Thiolate-Protected Au_{38} Nanocluster. *J. Am. Chem. Soc.* **2010**, *132*, 8210−8218.

(4) Hulkko, E.; Lopez-Acevedo, O.; Koivisto, J.; Levi-Kalisman, Y.; Kornberg, R. D.; Pettersson, M.; Häkkinen, H. Electronic and Vibrational Signatures of the $Au_{102}(p\text{-MBA})_{44}$ Cluster. *J. Am. Chem. Soc.* **2011**, *133*, 3752−3755.

(5) Wu, Z.; Chen, J.; Jin, R. One-Pot Synthesis of $Au_{25}(SG)_{18}$ 2- and 4-nm Gold Nanoparticles and Comparison of Their Size-Dependent Properties. *Adv. Funct. Mater.* **2011**, *21*, 177−183.

(6) Pei, Y.; Zeng, X. C. Investigating the Structural Evolution of Thiolate Protected Gold Clusters from First-Principles. *Nanoscale* **2012**, *4*, 4054−4072.

(7) Zhang, Y.; Cui, X.; Shi, F.; Deng, Y. Nano-Gold Catalysis in Fine Chemical Synthesis. *Chem. Rev.* **2012**, *112*, 2467−2505.

(8) Ansar, S. M.; Perera, G. S.; Jiang, D.; Holler, R. a.; Zhang, D. Organothiols Self-Assembled onto Gold: Evidence for Deprotonation of the Sulfur-Bound Hydrogen and Charge Transfer from Thiolate. *J. Phys. Chem. C* **2013**, *117*, 8793−8798.

(9) Knoppe, S.; Dolamic, I.; Bürgi, T. Racemization of a Chiral Nanoparticle Evidences the Flexibility of the Gold-Thiolate Interface. *J. Am. Chem. Soc.* **2012**, *134*, 13114−13120.

(10) Varnholt, B.; Dolamic, I.; Knoppe, S.; Bürgi, T. On the Flexibility of the Gold-Thiolate Interface: Racemization of the $Au_{40}(SR)_{24}$ Cluster. *Nanoscale* **2013**, *5*, 9568−9571.

(11) Beqa, L.; Deschamps, D.; Perrio, S.; Gaumont, A.-C.; Knoppe, S.; Bürgi, T. Ligand Exchange Reaction on $Au_{38}(SR)_{24}$, Separation of $Au_{38}(SR)_{23}(SR')_1$ Regioisomers, and Migration of Thiolates. *J. Phys. Chem. C* **2013**, *117*, 21619−21625.

(12) Tlahuice-Flores, A.; Whetten, R. L.; Jose-Yacaman, M. Vibrational Normal Modes of Small Thiolate-Protected Gold Clusters. *J. Phys. Chem. C* **2013**, *117*, 12191−12198.

(13) Price, R. C.; Whetten, R. L. Raman Spectroscopy of Benzenethiolates on Nanometer-Scale Gold Clusters. *J. Phys. Chem. B* **2006**, *110*, 22166−22171.

(14) Parker, J. F.; Choi, J.; Wang, W.; Murray, R. W. Electron Self-Exchange Dynamics of the Nanoparticle Couple $[Au_{25}(SC_2Ph)_{18}]^{0/1-}$ by Nuclear Magnetic Resonance Line-Broadening. *J. Phys. Chem. C* **2008**, *112*, 13976−13981.

(15) Dolamic, I.; Varnholt, B.; Bürgi, T. Far-Infrared Spectra of Well-Defined Thiolate-Protected Gold Clusters. *Phys. Chem. Chem. Phys.* **2013**, *15*, 19561−19565.

(16) Farrag, M.; Tschurl, M.; Dass, A.; Heiz, U. Infra-Red Spectroscopy of Size Selected Au_{25}, Au_{38} and Au_{144} Ligand Protected Gold Clusters. *Phys. Chem. Chem. Phys.* **2013**, *15*, 12539−12542.

(17) Koivisto, J.; Salorinne, K.; Mustalahti, S.; Lahtinen, T.; Malola, S.; Häkkinen, H.; Pettersson, M. Vibrational Perturbations and Ligand−Layer Coupling in a Single Crystal of $Au_{144}(SC_2H_4Ph)_{60}$ Nanocluster. *J. Phys. Chem. Lett.* **2014**, *144*, 387−392.

(18) Gautier, C.; Taras, R.; Gladiali, S.; Bürgi, T. Chiral 1,1′-Binaphthyl-2,2′-Dithiol-Stabilized Gold Clusters: Size Separation and Optical Activity in the UV-Vis. *Chirality* **2008**, *20*, 486−493.

(19) Knoppe, S.; Boudon, J.; Dolamic, I.; Dass, A.; Bürgi, T. Size Exclusion Chromatography for Semipreparative Scale Separation of $Au_{38}(SR)_{24}$ and $Au_{40}(SR)_{24}$ and Larger Clusters. *Anal. Chem.* **2011**, *83*, 5056−5061.

(20) Qian, H.; Jin, R. Ambient Synthesis of $Au_{144}(SR)_{60}$ Nanoclusters in Methanol. *Chem. Mater.* **2011**, *23*, 2209−2217.

(21) Knoppe, S.; Kothalawala, N.; Jupally, V. R.; Dass, A.; Bürgi, T. Ligand Dependence of the Synthetic Approach and Chiroptical Properties of a Magic Cluster Protected with a Bicyclic Chiral Thiolate. *Chem. Commun.* **2012**, *48*, 4630−4632.

(22) Knoppe, S.; Bürgi, T. The Fate of $Au_{25}(SR)_{18}$ Clusters upon Ligand Exchange with Binaphthyl-Dithiol: Interstaple Binding vs. Decomposition. *Phys. Chem. Chem. Phys.* **2013**, *15*, 15816−15820.

(23) Hug, W.; Hangartner, G. A Novel High-Throughput Raman Spectrometer for Polarization Difference Measurements. *J. Raman Spectrosc.* **1999**, *30*, 841−852.

(24) Haesler, J. Construction of a New Forward and Backward Scattering Raman Optical Activity Spectrometer and Graphical Analysis of Measured and Calculated Spectra for (R)-[2H1,2H2,2H3]-Neopentane, Université de Fribourg, 2006; p 251.
(25) Brandt, N. N.; Brovko, O. O.; Chikishev, A. Y.; Paraschuk, O. D. Optimization of the Rolling-Circle Filter for Raman Background Subtraction. *Appl. Spectrosc.* **2006**, *60*, 288−293.
(26) Ahlrichs, R.; Bär, M.; Häser, M.; Horn, H.; Kölmel, C. Electronic Structure Calculations on Workstation Computers: The Program System Turbomole. *Chem. Phys. Lett.* **1989**, *162*, 165−169.
(27) Schäfer, A.; Horn, H.; Ahlrichs, R. Fully Optimized Contracted Gaussian Basis Sets for Atoms Li to Kr. *J. Chem. Phys.* **1992**, *97*, 2571−2577.
(28) Eichkorn, K.; Weigend, F.; Treutler, O.; Ahlrichs, R. Auxiliary Basis Sets for Main Row Atoms and Transition Metals and Their Use to Approximate Coulomb Potentials. *Theor. Chem. Acc.* **1997**, *97*, 119−124.
(29) Andrae, D.; Haussermann, U.; Dolg, M.; Stoll, H.; Preuss, H. Energy-Adjusted Ab Initio Pseudopotentials for the Second and Third Row Transition Elements. *Theor. Chim. Acta* **1990**, *77*, 123−141.
(30) Becke, A. D. Density-Functional Exchange-Energy Approximation with Correct Asymptotic Behavior. *Phys. Rev. A* **1988**, *38*, 3098−3100.
(31) Perdew, J. Density-Functional Approximation for the Correlation Energy of the Inhomogeneous Electron Gas. *Phys. Rev. B* **1986**, *33*, 8822−8824.
(32) Neugebauer, J.; Hess, B. A. Fundamental Vibrational Frequencies of Small Polyatomic Molecules from Density-Functional Calculations and Vibrational Perturbation Theory. *J. Chem. Phys.* **2003**, *118*, 7215.
(33) Luber, S.; Neugebauer, J.; Reiher, M. Intensity Tracking for Theoretical Infrared Spectroscopy of Large Molecules. *J. Chem. Phys.* **2009**, *130*, 064105.
(34) Luber, S.; Reiher, M. Theoretical Raman Optical Activity Study of the Beta Domain of Rat Metallothionein. *J. Phys. Chem. B* **2010**, *114*, 1057−1063.
(35) Luber, S.; Reiher, M. Calculated Raman Optical Activity Spectra of 1,6-Anhydro-Beta-D-Glucopyranose. *J. Phys. Chem. A* **2009**, *113*, 8268−8277.
(36) Eichkorn, K.; Treutler, O.; Öhm, H.; Häser, M.; Ahlrichs, R. Auxiliary Basis Sets to Approximate Coulomb Potentials. *Chem. Phys. Lett.* **1995**, *240*, 283−290.
(37) Casida, M. E. Time-Dependent Density-Funtional Theory for Molecules. In *Recent Advances in Density Funtional Response Theory for Molecules*; Chong, D. P., Ed.; World Scientific: Singapore, 1995; pp 155−192.
(38) Bauernschmitt, R.; Häser, M.; Treutler, O.; Ahlrichs, R. Calculation of Excitation Energies within Time-Dependent Density Functional Theory Using Auxiliary Basis Set Expansions. *Chem. Phys. Lett.* **1997**, *264*, 573−578.
(39) Wilson, E. B. *Molecular Vibrations: The Theory of Infrared and Raman Vibrational Spectra*; McGraw-Hill: New York, 1955.
(40) Neugebauer, J.; Reiher, M.; Kind, C.; Hess, B. A. Quantum Chemical Calculation of Vibrational Spectra of Large Molecules - Raman and IR Spectra for Buckminsterfullerene. *J. Comput. Chem.* **2002**, *23*, 895−910.
(41) Weymuth, T.; Haag, M. P.; Kiewisch, K.; Luber, S.; Schenk, S.; Jacob, C. R.; Herrmann, C.; Neugebauer, J.; Reiher, M. MOVIPAC: Vibrational Spectroscopy with a Robust Meta-Program for Massively Parallel Standard and Inverse Calculations. *J. Comput. Chem.* **2012**, *33*, 2186−2198.
(42) Bauernschmitt, R.; Ahlrichs, R. Treatment of Electronic Excitations within the Adiabatic Approximation of Time Dependent Density Functional Theory. *Chem. Phys. Lett.* **1996**, *256*, 454−464.
(43) Furche, F.; Ahlrichs, R. Adiabatic Time-Dependent Density Functional Methods for Excited State Properties. *J. Chem. Phys.* **2002**, *117*, 7433−7447.
(44) Bickley, W. G. Formulae for Numerical Differentiation. *Math. Gaz.* **1941**, *25*, 19−27.
(45) Fedorovsky, M. PyVib2, a Program for Analyzing Vibrational Motion and Vibrational Spectra, 2007.
(46) Hug, W. Visualizing Raman and Raman Optical Activity Generation in Polyatomic Molecules. *Chem. Phys.* **2001**, *264*, 53−69.
(47) Badawi, H. M. Vibrational Spectra and Assignments of 2-Phenylethanol and 2-Phenoxyethanol. *Spectrochim. Acta, Part A* **2011**, *82*, 63−68.
(48) Heaven, M. W.; Dass, A.; White, P. S.; Holt, K. M.; Murray, R. W. Crystal Structure of the Gold Nanoparticle $[N(C_8H_{17})_4][Au_{25}(SCH_2CH_2Ph)_{18}]$. *J. Am. Chem. Soc.* **2008**, *130*, 3754−3755.
(49) Qian, H.; Eckenhoff, W. T.; Zhu, Y.; Pintauer, T.; Jin, R. Total Structure Determination of Thiolate-Protected Au_{38} Nanoparticles. *J. Am. Chem. Soc.* **2010**, *132*, 8280−8281.
(50) Malola, S.; Lehtovaara, L.; Knoppe, S.; Hu, K.-J.; Palmer, R. E.; Bürgi, T.; Häkkinen, H. $Au_{40}(SR)_{24}$ Cluster as a Chiral Dimer of 8-Electron Superatoms: Structure and Optical Properties. *J. Am. Chem. Soc.* **2012**, *134*, 19560−19563.
(51) Jiang, D.-E. The Expanding Universe of Thiolated Gold Nanoclusters and Beyond. *Nanoscale* **2013**, *102*, 7149−7160.
(52) Lopez-Acevedo, O.; Akola, J.; Whetten, R. L.; Grönbeck, H.; Häkkinen, H. Structure and Bonding in the Ubiquitous Icosahedral Metallic Gold Cluster $Au_{144}(SR)_{60}$. *J. Phys. Chem. C* **2009**, *113*, 5035−5038.
(53) Gautier, C.; Bürgi, T. Vibrational Circular Dichroism of Adsorbed Molecules: BINAS on Gold Nanoparticles. *J. Phys. Chem. C* **2010**, *114*, 15897−15902.
(54) Molina, B.; Sánchez-Castillo, A.; Knoppe, S.; Garzón, I. L.; Bürgi, T.; Tlahuice-Flores, A. Structures and Chiroptical Properties of the BINAS-Monosubstituted $Au_{38}(SCH_3)_{24}$ Cluster. *Nanoscale* **2013**, *5*, 10956−10962.
(55) Knoppe, S.; Michalet, S.; Bürgi, T. Stabilization of Thiolate-Protected Gold Clusters Against Thermal Inversion: Diastereomeric $Au_{38}(SCH_2CH_2Ph)_{24-2x}(R\text{-BINAS})_x$. *J. Phys. Chem. C* **2013**, *117*, 15354−15361.